Salud, Ciencia y Tecnología. 2023; 3:434
doi: 10.56294/saludcyt2023434

ORIGINAL

Development of a New Algorithm for Classifying Cerebral Tumours Using MRI Images

Desarrollo de un nuevo algoritmo de clasificación de tumores cerebrales mediante imágenes de resonancia magnética

Bhavna Kaushik Pancholi[1], Pramodkumar Sevantilal Modi[1], Nehal Gitesh Chitaliya[1]

[1]The Maharaja Sayajirao University of Baroda. Department of Electrical Engineering. Vadodara, Gujarat, India

Citar como: Kaushik Pancholi B, Sevantilal Modi P, Gitesh Chitaliya N. Development of a New Algorithm for Classifying Cerebral Tumours Using MRI Images. Salud, Ciencia y Tecnología. 2023; 3:434. https://doi.org/10.56294/saludcyt2023434

Received: 20-04-2023 **Reviewed:** 16-05-2023 **Accepted:** 23-06-2023 **Published:** 24-06-2023

Editor: Fasi Ahamad Shaik, https://orcid.org/0000-0002-1216-5035

ABSTRACT

Healthcare scientists determined how MRI images have indeed been highly beneficial in latest times in the investigation of the recognition and early identification of a brain disease. The main primary stages in analysing the brain MRI pictures are image pre-processing, segmentation, feature extraction, and classification. Among the crucial processes that can evaluate how well brain MRI scans can be classified and ultimately the condition it will indicate is feature extraction and segmentation. In this paper stage wise methods are described. In the first stage (pre-processing stage) different filters; like; median, wiener, anisotropic, non-local means as well as combined filters used. In the pre-processing part, combined wiener and anisotropic filter gives the best result. In the second stage (segmentation stage), multi-thresholding technique – cuckoo search algorithm used using different objective functions; like; ostu, kapur entropy, tsallis entropy and proposed. In the proposed method of the segmentation stage used cuckoo search algorithm using combined ostu and tsallis entopy as an objective function. In the third stage (feature extraction), discrete wavelet transform used and in the fourth stage (classification) support vector machine used. In each stage results are compared using different parameters and we got best output using proposed method.

Keywords: MRI Images; Brain Tumour; Pre-Processing; Image Segmentation; Feature Extraction.

RESUMEN

Los científicos sanitarios han determinado que las imágenes de resonancia magnética han sido muy beneficiosas en los últimos tiempos para la investigación del reconocimiento y la identificación precoz de enfermedades cerebrales. Las principales etapas primarias en el análisis de las imágenes de resonancia magnética del cerebro son el preprocesamiento de imágenes, la segmentación, la extracción de características y la clasificación. Entre los procesos cruciales que pueden evaluar lo bien que se pueden clasificar las imágenes de resonancia magnética del cerebro y, en última instancia, la enfermedad que indicarán, se encuentran la extracción de características y la segmentación. En este artículo se describen métodos por etapas. En la primera etapa (etapa de preprocesamiento) se utilizan diferentes filtros, como la mediana, wiener, anisotrópico, medios no locales, así como filtros combinados. En la parte de preprocesamiento, los filtros wiener y anisotrópico combinados dan el mejor resultado. En la segunda etapa (etapa de segmentación), la técnica de umbralización múltiple - algoritmo de búsqueda de cuco utilizado utilizando diferentes funciones objetivas; como; ostu, kapur entropía, tsallis entropía y propuso. En el método propuesto de la etapa de segmentación utilizado cuckoo algoritmo de búsqueda utilizando ostu combinado y tsallis entropía como función objetivo. En la tercera etapa (extracción de características), transformada wavelet discreta utilizada y en la cuarta etapa (clasificación) máquina de vectores soporte utilizado. En cada etapa se comparan los resultados utilizando diferentes parámetros y se obtienen los mejores resultados utilizando el método propuesto.

Palabras clave: Imágenes De Resonancia Magnética; Tumor Cerebral; Preprocesamiento; Segmentación De Imágenes; Extracción De Características.

INTRODUCTION

One of the difficult problems in image processing is noise elimination, which deals with the restoration and image improvement of a digital image which has become distorted by noise during gathering, preservation, or dissemination. It is an unavoidable effort to eliminate or at least reduce noise in pictures. Perhaps a small amount of sound is harmful if higher efficiency is needed, as in the medical industry.[1]

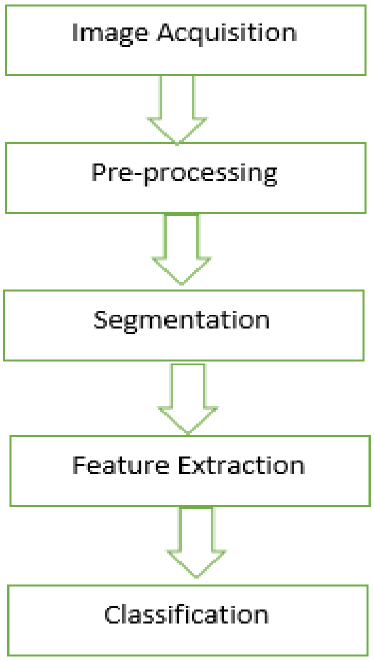

Figure 1. Block diagram of the proposed system

Figure 1 indicates stage wise block diagram of the proposed system. Stage wise survey given in the section 1.1 to 1.5. Stage wise theoretical aspects given in the section 2. Stage wise results given in the section 3. Conclusion given in the Section 4.

IMAGE ACQUISITION

The primary widely used diagnostic tools are medical images generated from ultrasound (US) imaging, MRI and CT scan and due to its non-invasive, safe, and precise nature. Furthermore, photo collection and equipment may bring up unwanted interruptions like speckle distortion, salt and pepper, Poisson and Gaussian noises. Due to the drastic degradation of optical measurements, like image density and intensity, it is difficult to distinguish among regular and diseased cells in medical studies. Therefore, a necessary pre-processing step to achieve the best evaluation is to denoise medical data without changing limits, modifying essential parts of the images, or harming anatomical traits. Brain tumours and other cerebral abnormalities can be diagnosed, graded, treated, and the effectiveness of the therapies can be evaluated using magnetic resonance imaging (MRI).[2] The morphological and physiological features of disorders in the neuraxis are revealed by standard MRI, but its accuracy is constrained. Although with current advancements in image accuracy, stronger electromagnetic fields, and better contrasted agents, standard imaged techniques still have a constrained ability to characterise tissue. Clients will have intrusive brain abnormalities biopsy procedures due to diagnostic uncertainty that carries some risk. The biophysical characteristics of brain tissue may now be statistically measured in vivo using a variety of supplemental MR imaging approaches, improving our understanding of regional variations in the cell micro - structural context. The methods included magnetic resonant spectroscopic, perfusion-weighted imaging, and diffusion-weighted imaging (MRS). The T1- and T2-weighted images are the least popular MRI procedures. Short TE and TR timings are used to create T1-weighted pictures. T1 characteristics of tissue are primarily responsible for determining the contrast and luminance of the picture. On the other hand, longer TE and TR periods are used to create T2-weighted pictures. In order to create this, lengthier TE and TR durations were used. The T2 characteristics of tissue are primarily responsible for determining the clarity and intensity of pictures. T1- and T2-weighted pictures may typically be distinguished simply by examining the CSF. On T1-weighted imaging, CSF is dark, while on T2-weighted imaging, it is bright. The Fluid Attenuated Inversion Recovery phase is a third frequently used technique (Flair).[3] The TE and TR timings of the Flair sequence are significantly longer than those of a T2-weighted image. As a result, anomalies are kept light, while the typical CSF fluid is dimmed. This sequence greatly facilitates the distinction among CSF and an abnormal and is highly susceptible to disease. Gadolinium infusion can also be used to produce T1-weighted imaging (Gad). A non-toxic diamagnetic contrast-enhancing compound is called Gad. Gad shortens T1 and alters signal intensity when administered within the scanning. Gad appears highly bright on T1-weighted pictures as a result. Gad enriched pictures are particularly helpful for examining vascular architecture and blood-brain membrane degradation. The purpose of diffusion weighted imaging (DWI) is to identify the erratic motions of water protons. In contrast to the intracellular region, where their migration is severely constrained, water molecules distribute quite easily in the external environment. Distribution, which refers to random motions, immediately becomes constrained in ischemic brain tissue. The sodium-potassium pump malfunctions during ischemia, causing intracellular sodium accumulation. The osmotic gradient then causes water to move from the extracellular to the intracellular area. This causes a very strong signal on the DWI as intracellular water flow is constrained. DWI is a highly accurate approach for identifying severe stroke. In this paper MRI images for brain tumour detection is used.

PRE-PROCESSING

In order to reduce distortion from an MRI image, I. Nagarajan's technique uses a block distinction processing mechanism. It works by adjusting each pixel's weight efficiently, separating edge pixels from noise pixels, and then reducing noise more precisely. Additionally, the method is evaluated on real T1 and T2 MRI scans in longitudinal, sagittal, and coronal viewpoints in addition to T1, T2, and PD feature generated MRI data. This method can be used to predict the processing time of MRI images for clinical clients in the future, and the accuracy of the suggested method can be improved by utilising an angular rotation-based block contrast approach.[4] The optimal filtering strategy for image pre-processing, which may have a significant impact on the accuracy of tumor cell detection, can be found by comparing Wiener and Median filtration strategies. The result of the Wiener filter determined the average and variable value of the images at a certain phase. The front and back of the threshold were distinguished using the grey-scale method. The deformation in the photographs is successfully removed by the median filter. The findings of the investigation in the previous study do not render the analysis's findings erroneous. The effectiveness of the filters is measured by whether effectively it examines images of blood platelets. The metric used to evaluate the filter's effectiveness was PSNR.[5]

The median filter performed best when the real picture is compared to the de-noised picture, demonstrating that it is a suitable fit for the small picture set employed in the study. For the provided data gathering, the wiener filter was compared to the median filter, and it was found that the median filter functioned 8 % better.

SEGMENTATION

The categorization of brain tumours is a difficult issue in the realm of clinical picture analysis. The current research suggests a hybrid approach that makes use of neuro-physics and convolutional neural networks (NS-CNN).[6,7,8] It seeks to distinguish between harmless and harmful tumour regions in sections separated from brain pictures. Initially, the neutrosophic group - master greatest fuzzy-sure entropy (NS-EMFSE) method was used to divide the MRI pictures. During the classification phase, CNN collected the characteristics of the fragmented brain pictures and evaluated those utilizing SVM and KNN algorithms. On 80 benign tumors and 80 malign tumors, an operational assessment predicated on 5-fold cross-validation is conducted. The results showed that CNN characteristics have excellent classification performance across a range of classifications.[9, 10]

While modelling findings verified source information with a mean accuracy rate of 95,62 %, actual findings show that CNN characteristics demonstrated superior categorization efficiency with SVM. By identifying brain tumors as harmless and malignant, the primary objective of this article is to develop an effective automated brain tumor separation method. NS-EMFSE was used to separate brain tumors. Alexnet collected the characteristics of the divided pictures using CNN structures, and SVM and KNN classifiers being used to determine their classification. The deep learning technique that uses feed-forward layers is CNN. The application utilized Matlab 2017b and the MatConvnet library. SVM classifier produced the best results, scoring 95,62 %.[11,12]

If more photos are utilized in the collection, it is predicted that this reliability percentage would rise. Research on segmentation and classification is among the least often discussed subjects in picture analysis. The renowned and effective segmentation and classification techniques CNN and Neutrosophy can be used, and this could significantly advance picture recognition. I intend to look into how distinct Neutrosophic methods using various CNN topologies affect classification reliability in upcoming research. Depending on a convolutional neural network with neutrosophic professional maximum fuzzy sure entropy, a brain tumor identification algorithm.

FEATURE EXTRACTION

Every photo software must use feature extraction and picture pre-processing methodologies. To guarantee the effectiveness of the following stages, these approaches should have a very large precision and resolution rate. However, these strategies' importance is frequently overlooked, that yields subpar outcomes. The significance of those methods is addressed in this research within the perspective of categorization and segmentation of Magnetic Resonance (MR) brain images. The removal of the skull section around the brain cells is accomplished in this research using appropriate pre-processing procedures. In the study, texture-based feature extracting methods are further demonstrated.(13)

The research findings are examined in respect of feature extracting strategies and separation effectiveness for pre-processing. In this study, the converging probability of different techniques is additionally covered. The outcomes of the experiments are encouraging for the suggested strategies. This research validates the value of feature extraction and pre-processing approaches. The presented methods have a very excellent reliability rate. The fact that the time commitment is relatively minimal shows that these strategies are doable. Therefore, these methods can be applied to real medical situations in which precision and resolution rate are crucial.

CLASSIFICATION

Brain tumors grow when cells arise abnormally. It is one of the leading causes of adult mortality worldwide. Early brain tumor discovery may avert countless of fatalities. Magnetic Resonance Imaging (MRI) earlier brain tumor detection can improve client life. The tumor is very readily seen in an MRI, which aids in the course of additional therapy. The research tries to identify tumors earlier on. Methodologies: In the paper, the input slices are enhanced and de-noised using a Weiner filter using several wavelet bands. Using the help of Potential Field (PF) categorization, tumor pixel subgroups are discovered. Additionally, in Fluid Attenuated Inversion Recovery (Flair) and T2 MRI, the tumor zone is isolated using a worldwide threshold and several statistical morphological techniques.

Local Binary Pattern and Gabor Wavelet Transform characteristics are combined for precise categorization. Results: The PSNR, MSE and SSIM are used to test the suggested technique. The outcomes are 76,38, 0,037, and 0,98 on T2 and 76,2, 0,039, and 0,98 on Flair, accordingly. Using the basis of pixels, distinct characteristics, and fused functionalities, the classification outcome has been assessed. The suggested method is compared with ground fact slices at the pixel level and validated in respect of foreground, background, and error region and pixel clarity.(14)

THEORETICAL ASPECT OF TECHNIQUES

In the pre-processing part, there are several filters used for noise removal, like; Median, Wiener, Anisotropic Diffusion filter, Non Local Means, etc.(15,16) Using an estimate of the necessary noise-free signal, the Wiener filter is frequently used in this to reduce the amount of distortion in a scan. It uses a statistical method. The Wiener filter is popular and produces high-quality results when compared to other filters because of how quickly and easily it can be implemented. Additionally, combining various filters yields results that are more accurate. In this paper different combination of the combined filters are used for pre-processing of an image; like; combined Weiner and anisotropic, combined Weiner and median, combined Weiner and non-local means. In this combined Weiner and anisotropic gives best output.

There are so many techniques are used for image segmentation. In this thresholding is the one of the technique used for image segmentation.(17) There are two types of thresholding; one is bi-level thresholding and other is multi-level thresholding.(18) Compare to the bi-level thresholding technique, multi-level thresholding techniques gives good performance. There are so many different algorithm are used in the multi-level thresholding techniques.(3) One of the algorithms is cuckoo search algorithm. In the cuckoo search algorithm, different objective functions are used for optimum output.(19)

CUCKOO SEARCH (CS) ALGORITHM

The cuckoo search algorithm was proposed by Yang.(10) and is a naturalistic method. The CS imitates the cuckoo's egg-laying operation. Cuckoos typically lay their fertilised eggs in host nests in the hopes that they would be nurtured by substitute parents in spring. The host may recognise that the eggs in their nests are not their own occasionally. In these situations, either the entire nest is thrown out or the foreign eggs are removed from the nests. The CS optimization algorithm is generally based on the following three principles:

1. It's interesting to note that each cuckoo bird only lays one egg at a time, which it randomly inserts in the nest of a host bird.
2. Typically, the best nests with top-notch eggs are passed down to the following generations.
3. There are a fixed number of host nests available. With probability p_{α}, the host bird finds foreign eggs with a probability that ranges from 0 to 1. Keep in mind that the best nests are chosen for the subsequent

calculations. For the sake of simplicity, principle 3 can be described as follows: with probability p_α, new nests will replace the existing n nests.

The CS method can be distilled into the following three ideas based on these three principles:

A Lévy light is carried out while producing new solution x_i^{t+1} for cuckoo I[10]

$$x_i^{t+1}= x_i^t+ \alpha_0 \ (x_i^t-x_{best}) \oplus Levy(\lambda)\text{........ } (1)$$

Where x_{best} denotes the current best solution, Element-wise multiplication, and α_0 is the step size $\alpha_0> 0$.

Levy flights are selected using a Levy distribution, which is given by:

$$Levy(\lambda) \sim u=t^{-\lambda},(1<\lambda\leq 3)\text{......... } (2)$$

Based on the breeding behaviour of several cuckoo species, we have developed a new metaheuristic called Cuckoo Search in conjunction with L'evy flights in this work. Show that CS is better than other metaheuristic algorithms based on the literature review. Studying multiobjective optimization applications is a simple extension of the possibly effective optimization method. Levy step size and x_{best} are the main challenges of the cuckoo search algorithm. x_{best} is found using optimization. Different methods are used to maximize the function, like; using Ostu's method, using Kapur entropy method, using Tsallis entropy method, etc.[20]

PROPOSED CUCKOO SEARCH (CS) ALGORITHM

Otsu's presumption of binary classes is its major drawback: The grayscale histogram is divided into two classes. However, in real-world segmentation problems we most generally deal with images having more than two classes of segments. According to the literature review, employing the Otsu approach for CS results in lower PSNR values than utilising Kapur's entropy. Because Tsallis entropy is non-extensive, when two identical systems unite, the combined system's entropy is not equal to the sum of the entropies of its subsystems. Compare to CS using Kapur's entropy method Tsallis entropy gives higher PSNR values and other parameters. The long-range correlations in an image can be described using the non-extensive entropy technique.[20] The range of its use is constrained by the fact that, like other entropy-based algorithms, it is still extremely sensitive to the disturbance of signals. For small target extraction, the Otsu method is more reliable but less precise. The benefits of the two can thus be combined to create a new algorithm with a broader range of applications. We proposed new method, combined Otsu and Tsallis entropy as an objective function to find the x_{best}.

The long-range correlations in an image can be described using the non-extensive entropy technique. The range of its use is constrained by the fact that, like other entropy-based algorithms, it is still extremely sensitive to the disturbance of signals. For small target extraction, the Otsu method is more reliable but less precise. The benefits of the two can thus be combined to create a new algorithm with a broader range of applications. Noting that information redundancy now governs the non-extensive parameter q in Tsallis entropy and cannot be set arbitrarily.

A new objective function is denoted by:

$$\mu(t)=S_q^{a+b} - (\sigma_W^2\ )^{1-q}\text{........ } (3)$$

q > 0 needs to be met in order to maintain the concavity of Tsallis entropy.[10] In contrast, q < 1 is referred to as superextensivity, which raises the system's overall entropy in compared to the extensive case (q = 1).[21] Practically speaking, practically all kinds of images display the superextensivity feature.[22] Consequently, 0 < q < 1 can be the appropriate range for the non-extensive parameter. We can see that each of the two strategies is designed to maximise the objective functions... Equations 3's goal is to increase the objective function.

$$t\text{^*}=Argmax\{\mu(t)\}\text{ .... } (4)$$

With the range of q stated above, equation 4 yields the ideal threshold. The profile of each peak is the normalised q-Gaussian distribution function for a synthetic image with a bimodal histogram distribution, as shown in figure 2.[6] We can see that the best threshold for the Otsu algorithm and the Tsallis entropy algorithm is the valley gray-level between the two peaks, which exactly matches the outcome of equation 4.[23] There is no proof that the result of ostu and tsallis entropy coincide for other natural photographs with an arbitrary histogram distribution, however equation 3 shows a trade-off between them and equation 4 may produce an appropriate proposal. It should be noted that S_q^{a+b} and σ_W^2 have extremely different magnitudes in the histogram of figure 2. Both of them are functions of threshold t, as illustrated in figure 3. The Otsu method, however, completely suppresses the Tsallis entropy algorithm's outputs for any conceivable threshold.[24] Consequently, it is inappropriate to directly combine S_q^{a+b} and σ_W^2.

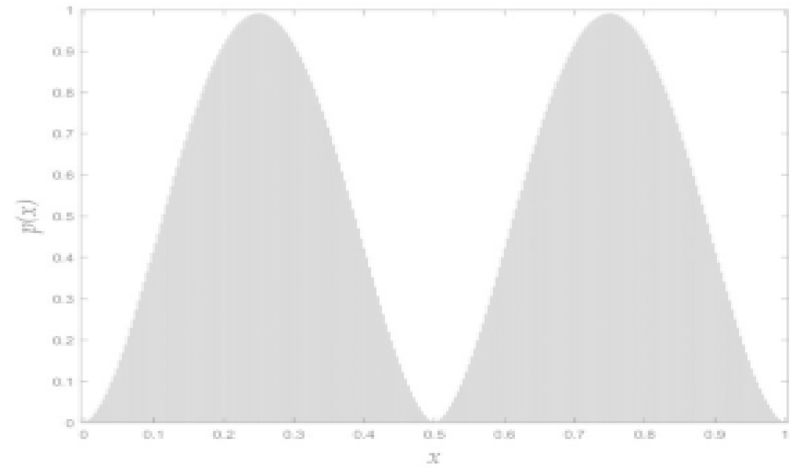

Figure 2. Normalized histogram distribution

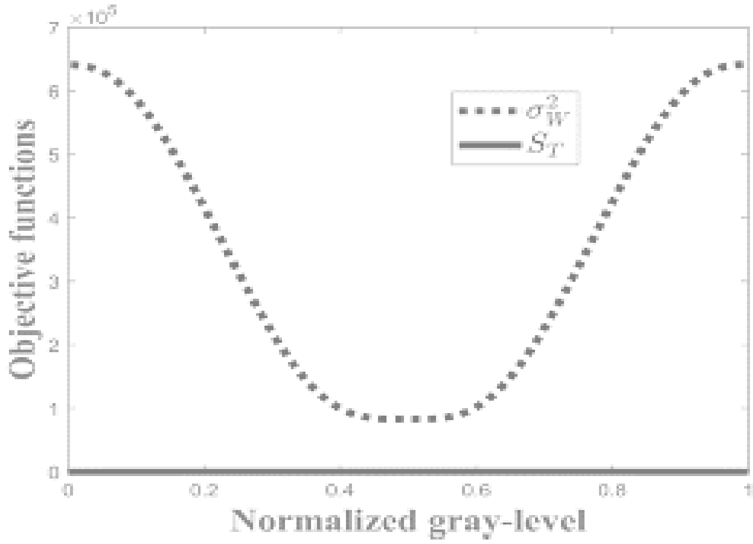

Figure 3. Objective functions of the Ostu and Tsallis algorithms

The magnitude of can be revised using the q-exponential function[20] to minimise the effects of the magnitude difference. With a continuous probability distribution function, Tsallis entropy is defined as:

$$S_T = \frac{1-\int_0^1 p(x)^q\,dx}{(q-1)} \quad \text{...... (5)}$$

Where the probability density of the normalised gray-level value is denoted by p(x). The appropriate probability distribution for a system with non-extensive q-entropy can be expressed as the q-Gaussian function[25],

$$p(x) = \frac{1}{Z_q}\left[1-(1-q)\frac{x^2}{\sigma^2}\right]^{\frac{1}{1-q}} \quad \text{........ (6)}$$

If Zq is the partition function to maintain the probability normalisation requirement and is the variance of x,

$$Z_q = \int_0^1 \left[1-(1-q)\frac{x^2}{\sigma^2}\right]^{\frac{1}{1-q}} dx = \frac{\sigma\sqrt{\pi}\,\Gamma\left(1+\frac{1}{1-q}\right)}{2\sqrt{1-q}\,\Gamma\left(\frac{3}{2}+\frac{1}{1-q}\right)} \quad \text{........ (7)}$$

Where factorial (k - 1)! will be reached from the Gamma function Γ(k) assuming k is a number. Adding p(x) to equation 18 results in:

$$S_T = \frac{1-\int_0^1 \frac{1}{x_q^q}\left[1-(1-q)\frac{x^2}{\sigma^2}\right]^{\frac{q}{1-q}} dx}{q-1} = \frac{\xi\left(\sigma^2\right)^{\frac{1-q}{2}}}{q-1} \quad \text{........ (8)}$$

Where:

$$\xi = \left[\frac{\pi}{4(1-q)}\right]^{\frac{1-q}{2}} \left[\frac{\Gamma\left(\frac{3}{2}+\frac{1}{1-q}\right)}{\Gamma\left(1+\frac{1}{1-q}\right)}\right]^{q} \frac{\Gamma\left(\frac{1}{1-q}\right)}{\Gamma\left(\frac{3-q}{2(1-q)}\right)} \quad \text{........ (9)}$$

Is the integration constant for a given value of q. According to the non-extensivity of Tsallis entropy, if If p_a and p_b are two identical q-Gaussian distribution functions, the total entropy can be expressed as follows:

$$S_T(a+b) = S_T(a) + S_T(b) + (1-q)S_T(a)S_T(b)$$

$$S_T(a+b) = \frac{1-\xi_a\left(\sigma_a^2\right)^{\frac{1-q}{2}}}{q-1} + \frac{1-\xi_b\left(\sigma_b^2\right)^{\frac{1-q}{2}}}{q-1} + (1-q)\frac{1-\xi_a\left(\sigma_a^2\right)^{\frac{1-q}{2}}}{q-1}\frac{1-\xi_b\left(\sigma_b^2\right)^{\frac{1-q}{2}}}{q-1} \quad \text{..... (10)}$$

Substituting $\sigma_a^2 = \sigma_b^2 = \sigma_W^2$ into equation 23 yields:

$$S_T(a+b) = \frac{1-\xi_a\xi_b\left(\sigma_W^2\right)^{1-q}-1}{1-q} \quad \text{....... (11)}$$

Therefore, the magnitude of $(\sigma_W^2)^{1-q}$ is comparable with S_T(a+b) at the proper range of q, and the rationality of equation 3 is shown.

RESULT ANALYSIS

PRE-PROCESSING

The description of parameters implemented for 7 images is given below[1]

PEAK SIGNAL TO NOISE RATIO (PSNR)

The PSNR is the proportion of utmost attainable signal intensity to distorted noise signal intensity. The statistic used to evaluate it is the decibel (dB). It is the most often used quality assessment metric for distorted photographs that have been rebuilt. [26] The signal, which is the real data, gets reduced or deformed as a result, and this results in noise. PSNR is displayed as:

$$\mathrm{PSNR} = \frac{10 \log 255^2}{\mathrm{MSE}} \quad \text{......... (12)}$$

MEAN SQUARE ERROR (MSE)

Among the two monochrome images P and Q, one is real and the other is contrived. The input image, pij, and the filtered output image, qij, are both M x N in dimension. Summarizing the values of I and j represents the total number of pixels in the images, whereas M and N represent the number of rows and columns in the primary images.[26] MSE is used to determine the mean of the squares of the variance in a source and screened scan. The dimension is at its smallest when the photographs are nearly similar. The more MSE there are, the better it is for figuring out how much the image has improved.

$$\mathrm{MSE} = \frac{\sum_{j=1}^{N}\left(\sum_{i=1}^{M}\left(p_{ij}-q_{ij}\right)^2\right)}{MN} \quad \text{....... (13)}$$

ROOT MEAN SQUARE ERROR (RMSE)

RMSE is a widely used inaccuracy measuring tool. It is a method that figures out the difference among the actual and predicted results.[26]

The final RMSE score frequently conveys the degree of the variation's severity and is unfavourable. The square root of MSE is RMSE. If RMSE is below a given threshold, performance is increased.

$$\mathrm{RMSE} = \sqrt{\mathrm{MSE}} \quad \text{........ (14)}$$

UNIVERSAL QUALITY INDEX (UQI)

A statistic is described as "global" since it is unaffected by the conditions under which it was observed. The ideal outcome although is 1 and the dynamic scale is [-1, 1]. It corrects for incoherence, brightness distortion, and intensity disturbance in one parameter.[26] Assume that $p = \{p_i \mid i = 1,2, \ldots \ldots N\}$ and $q = \{q_i \mid i = 1,2, \ldots \ldots N\}$ is the real and assessed image values, respectively. According to the suggested quality index's description:

$$\mathrm{UQI} = \frac{4\sigma_{pq}\,\overline{pq}}{\left(\sigma_p^2+\sigma_q^2\right)\left(\overline{p}^2+\overline{q}^2\right)} \quad \text{........ (15)}$$

here,

$$\overline{p} = \frac{1}{N}\sum_{i=1}^{N} p_i \,, \overline{q} = \frac{1}{N}\sum_{i=1}^{N} q_i$$

$$\sigma_p^2 = \frac{1}{N-1}\sum_{i=1}^{N}(p_i - \overline{p})^2, \sigma_q^2 = \frac{1}{N-1}\sum_{i=1}^{N}(q_i - \overline{q})^2$$

$$\sigma_{pq} = \frac{1}{N-1}\sum_{i=1}^{N}(p_i - \overline{p})\,(q_i - \overline{q})$$

In the research work implementation of the specific filters as well as the combining of filters is employed. The PSNR that is measured in dB and represents the best possible signal-to-deformed-noise ratio ought to be higher in value. To calculate PSNR, various filters such as Median, Weiner, Anisotropic, Non-Local Median (NLM), and filter combinations are utilised. Of all the individual filters, the Weiner filter produced the best results. It was therefore continued for further filter combinations.

Figure 4 reflects the mean result for five distinct cases of each filter. The Mean result of the Median Filter was 30,15801 dB, the Weiner filter is 35,20005 dB, the anisotropic filter was 32,3954 dB and the NLM filter was 30,73707 dB. The mean result of Weiner and NLM was 35,95141 dB, Weiner and Anisotropic was 37,37613 dB and Weiner and Median was 35,88817 dB while taking into account the combination of filters.

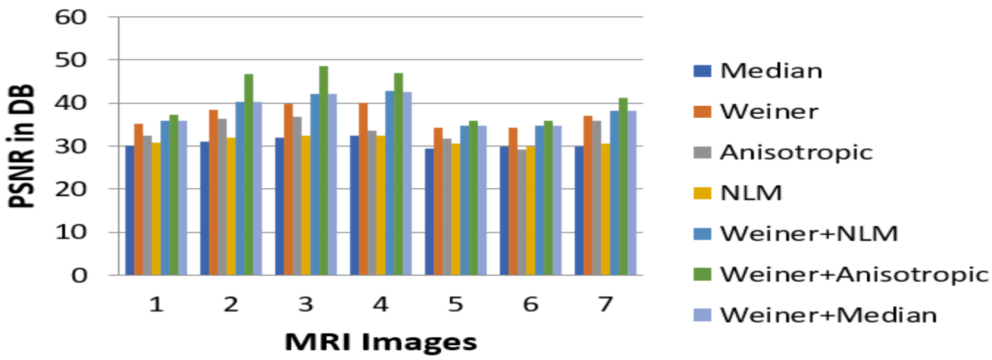

Figure 4. MRI Image of the PSNR in dB for Median filter, Weiner filter, Anisotropic filter, NLM, Weiner and NLM, Weiner and Anisotropic and Weiner and Median

MSE is used to determine the mean square of errors for both the actual and intended scans. The MSE value, which is determined in dB, must be as low as possible to obtain an accurate image. In figure 5, the MSE for each separate filter is determined, and the mean values for five distinct cases is shown. The Median filter had a Mean value of 63,19438 dB, Weiner filter of 19,79131 dB, Anisotropic filter of 37,75201 dB and NLM filter of 55,30606 dB. The mean result of Weiner and NLM was 16,64712 dB, Weiner and Anisotropic was 11,99131 dB, and Weiner and Median was 16,89131 dB when the combination of filters was taken into account.

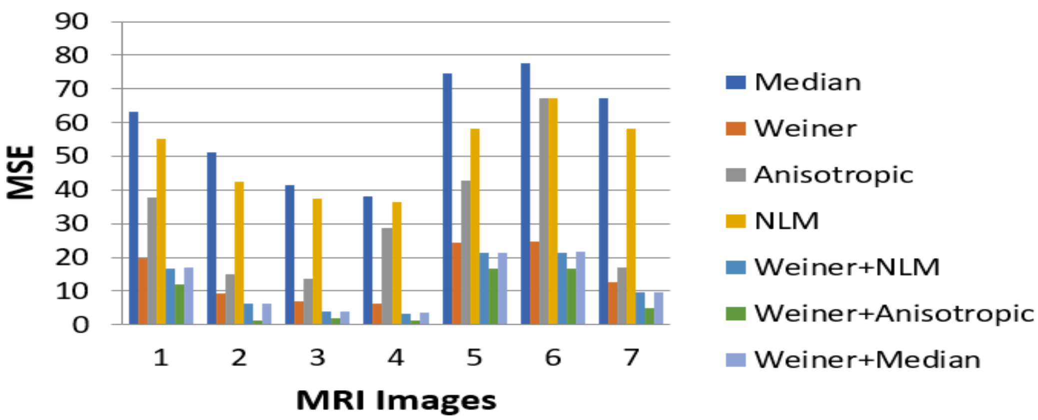

Figure 5. MRI Image of the MSE in dB for Median filter, Weiner filter, Anisotropic filter, NLM, Weiner and NLM, Weiner and Anisotropic and Weiner and Median

https://doi.org/10.56294/saludcyt2023434

It is common procedure to quantify inconsistency using the Root Mean Squared Error (RMSE), which is calculated in dB and must be kept to a low to ensure good output. Figure 6 shows the RMSE for each unique filter and the mean result for five distinct cases. The Mean values of the Median filter, Weiner filter, Anisotropic filter and NLM filter was 7,94949 dB, 4,44874 dB, 7,4368 dB and 6,14427 dB, respectively. Weiner and NLM had a mean value of 4,08009 dB, Weiner and Anisotropic had a value of 3,46285 dB, and Weiner and Median had a value of 4,1099 dB when the combination of filters is taken into account.

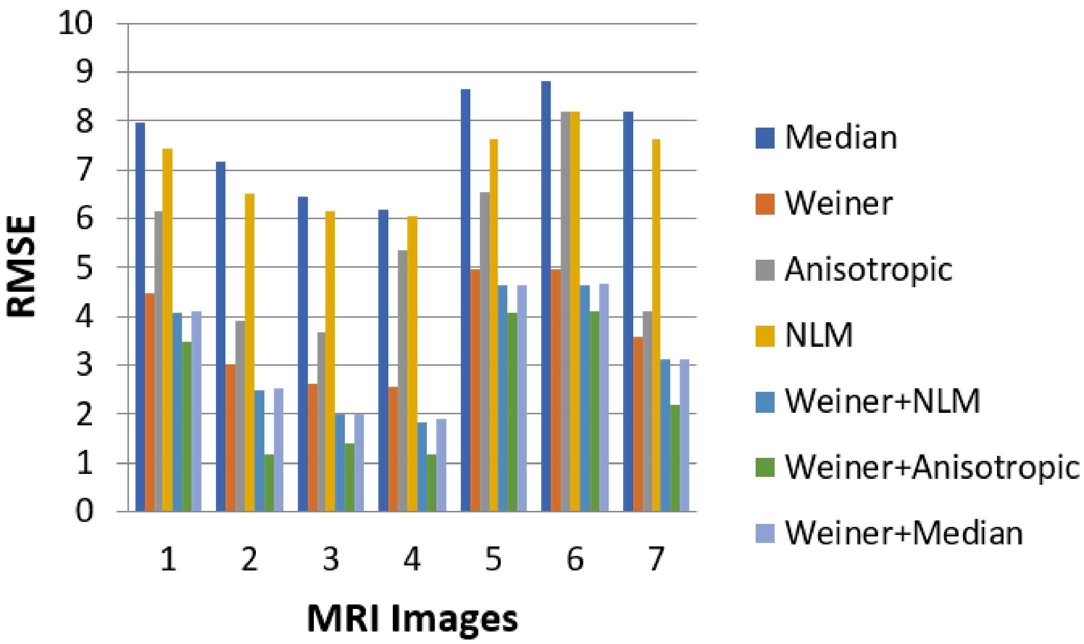

Figure 6. MRI Image of the RMSE in dB for Median filter, Weiner filter, Anisotropic filter, NLM, Weiner and NLM, Weiner and Anisotropic and Weiner and Median

The Universal Image Quality Index (UQI) of the filter is evaluated in dB and is ought to be higher for improved noise - reducing quality. The single filter and mean values for five separate cases is shown in figure 7. The Mean values of the Median Filter, Weiner Filter, Anisotropic Filter and NLM Filter was 0,7293 dB, 0,91696 dB, 0,92288 dB and 0,68378 dB respectively. The Mean result of Weiner and NLM was 0,92966 dB, Weiner and Anisotropic was 0,96896 dB, and Weiner and Median was 0,92896 dB when the combination of filters was taken into account.

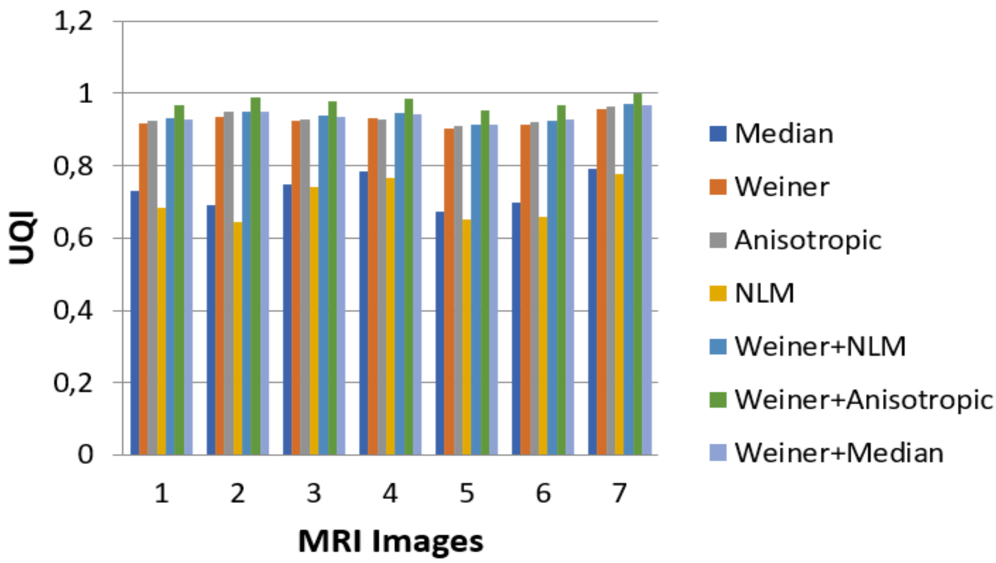

Figure 7. MRI Image of the UQI in dB for Median filter, Weiner filter, Anisotropic filter, NLM, Weiner and NLM, Weiner and Anisotropic and Weiner and Median

SEGMENTATION

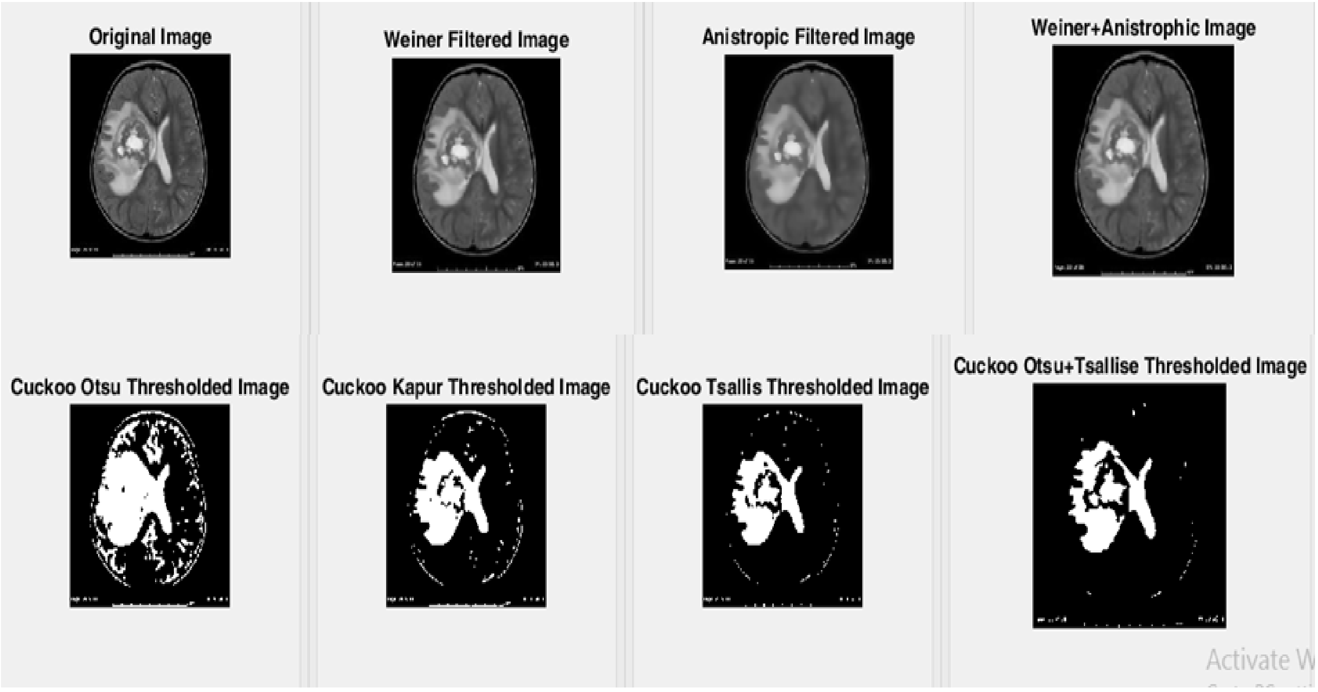

Figure 8: Pictorial Presentation of Pre-processing and Segmentation output of Weiner Filter, Anistropic Filter, Weiner Filter & Anistropic Filter, Cuckoo Ostu Threshold, Cuckoo Kapur Threshold, Cuckoo Tsallis Threshold and Cuckoo Otsu & Tsallise Threshold

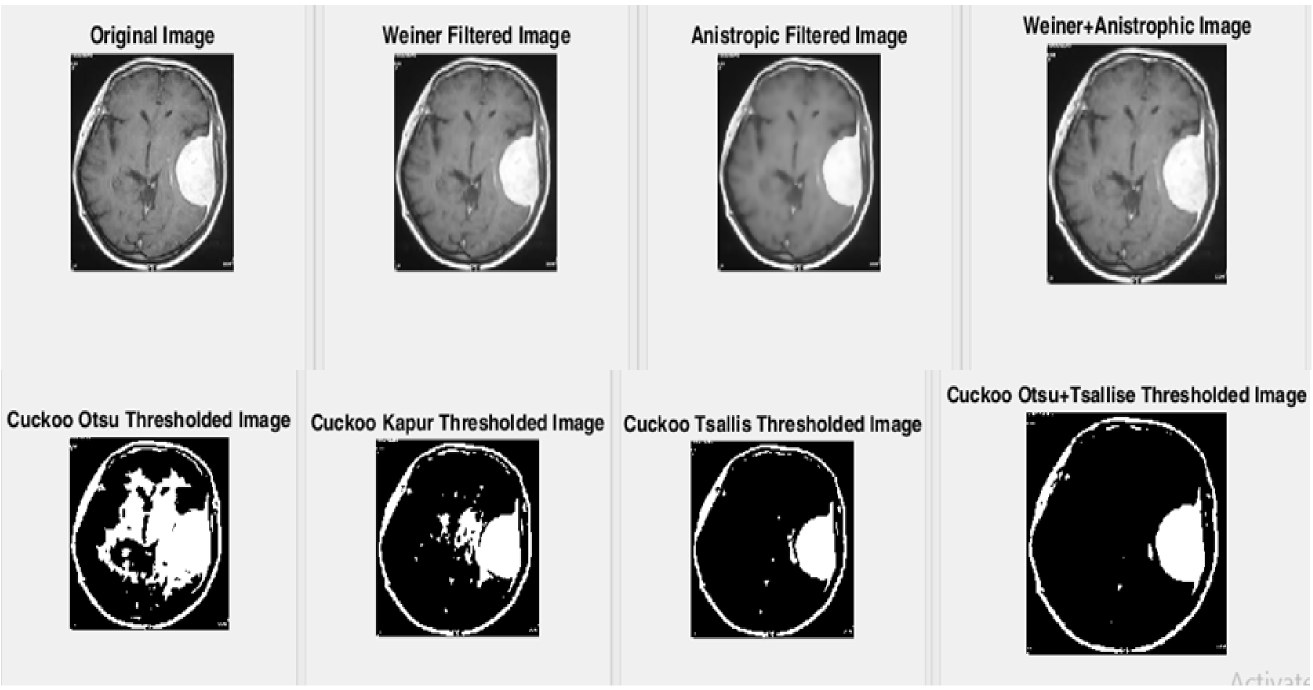

Figure- 9: Pre-processing and Segmentation Output Images of Weiner Filter, Anistropic Filter, Weiner Filter & Anistropic Filter, Cuckoo Ostu Threshold, Cuckoo Kapur Threshold, Cuckoo Tsallis Threshold and Proposed method

Pre-processing and Segmentation image samples are shown in figures 8 and 9. The Weiner Filter, Anistropic Filter and Weiner Filter & Anistropic Filter Pictorial Presentation is displayed in the front row of figures 5 and 6. These filters are described theoretically in the section 3 along with their parameters like PSNR, MSE, RMSE & UQI with their equations. The segmentation output, which includes the Cuckoo Ostu Threshold, Cuckoo Kapur Threshold, Cuckoo Tsallis Threshold and Cuckoo Otsu & Tsallis Threshold is vividly represented. The proposed research demonstrates that when compared to various individual and combined filters, the Cuckoo Otsu &

Tsallis entropy combination produces outstanding outcomes.

FEATURE EXTRACTION

The description of parameters implemented for 7 images is given below[8]

MEAN

The intensity of a grey magnitude picture is typically measured statistically using the term mean.[9]

$$\mathrm{Mean} = \frac{1}{m+n}\sum_{x=0}^{m-1}\sum_{y=0}^{n-1} f(x,y) \quad \text{....... (16)}$$

STANDARD DEVIATION

This variable displays the degree of "diffusion" from the median or anticipated intensity of the pixel. The significant standardized variation signifies that the data units are dispersed relatively randomly, whereas a low standardized variation indicates that the data units have a tendency to be near the mean.[14]

The Standard Deviation is given by:

$$\mathrm{StandardDeviation(SD)} = \sqrt{\frac{1}{m+n}\sum_{x=0}^{m-1}\sum_{y=0}^{n-1}(f(x,y)-\mathrm{Mean})^2} \quad \text{...... (17)}$$

VARIANCE

It evaluates neighbouring distinction and sums up the histogram dispersion.[21] The divergence and dispersion from the average are greater the more the variance.

$$\mathrm{Variance} = \sigma^2 = \sum_{x=0}^{m-1}\sum_{y=0}^{n-1}(x-\mu)^2(y-\mu)^2 . f(x,y) \quad \text{....... (18)}$$

ROOT MEAN SQUARE ERROR

It calculates the discrepancy among the observed value that a system or classifier anticipated and the real value.

$$\mathrm{MSE} = \frac{\sum_{j=1}^{N}\left(\sum_{i=1}^{M}(f_{ij}-y_{ij})^2\right)}{MN} \quad \text{..... (19)}$$

RMSE=√MSE...... (20)

ENTROPY

This relates to the amount of energy which is constantly dissipated to heat whenever a process or structural transition takes place; the idea derives from thermodynamics. When grey values are dispersed evenly, perhaps with identical possibilities, a picture's entropy is at its highest. Photos with minimal entropy have little content and poor picture resolution, whereas pictures with greater levels have more data and better features. Entropy can never be restored to be put to productive usage. As a result, the word might be interpreted as the degree of irreparable disarray or instability. The entropy of a grayscale picture can be described as:

$$\mathrm{Entropy} = \sum_{x=0}^{m-1}\sum_{y=0}^{n-1} f(x,y)\log_2 f(x,y) \quad \text{.... (21)}$$

SKEWNESS

It serves as a measure for symmetrical or, rather specifically, for asymmetry.[21] When a distributed or set of data appears identical to the left and right of the centre, it is said to be symmetrical.

$$S_K = \frac{1}{m+n}\sum\frac{(f(x,y)-\mathrm{Mean})^3}{SD^3} \quad \text{...... (22)}$$

KURTOSIS

It evaluates how heavy or light-tailed the information are in comparison to a statistical allocation.

$$K = \frac{1}{m*n}\sum\frac{(f(x,y)-\mathrm{Mean})^4}{SD^4} \quad \text{........ (23)}$$

ENERGY

It is consistency or angular second moment (ASM). The value increases with the homogeneity of the picture. The assumption is that the picture is a steady picture if energies is equivalent to 1.[21]

https://doi.org/10.56294/saludcyt2023434

$$\text{Energy} = \sqrt{\sum_{x=0}^{m-1}\sum_{y=0}^{n-1} f^2(x,y)} \quad \ldots\ldots (23)$$

CONTRAST

Brightness or grey-level differences among the standard pixel and its neighbour are measured as contrast. Contrast in the actual globe is created by the contrast between one element as well as other things in the identical range of sight in colour and intensity. The unit is located on the diagonal therefore x- y = 0 if x and y are identical. Assuming a value of 0, such data indicate pixels that are identical to its neighbour in every way. There is a slight difference and the value is 1 if x and y vary by 1. The contrast is rising and the magnitude is four if x and y are varied by two. As (x,y) rises, the weights tend to rise rapidly.[21]

$$\text{Contrast} = \sum_{x=0}^{m-1}\sum_{y=0}^{n-1} (x-y)^2 f(x,y) \quad \ldots\ldots.. (25)$$

CORRELATION

The co-occurrence matrix grey level elements linear dependence is demonstrated by the correlation characteristic. It shows how closely linked a baseline pixel is to its neighbour's. Here 0 indicates no connection and 1 indicates an ideal one.

$$\text{Correlation} = \frac{\sum_{x=0}^{m-1}\sum_{y=0}^{n-1}\big((x,y)f(x,y)\big) - M_X M_Y}{\sigma_X \sigma_Y}$$

INVERSE DIFFERENT MOMENT (IDM)

IDM is typically referred to as homogeneity which evaluates the regional homogeneity of a picture. The assessments of the dispersion of GLCM component's proximity to the GLCM diagonal are obtained by the IDM characteristic. Its value obtained is the opposite of a Contrast weight having values falling off the diagonal progressively.

$$\text{InverseDifferenceMoment(IDM)} = \sum_{x=0}^{m-1}\sum_{y=0}^{n-1} \frac{1}{1+(x-y)^2} f(x,y) \quad \ldots\ldots (27)$$

HOMOGENEITY

It analyses the resemblance of pixels. The homogeneity of a diagonally grey layer co-occurrence vector is 1.[21] If just little modifications are made to localize texturing, it expands in size.

$$\text{Homogeneity} = \sum_{x=0}^{m-1}\sum_{y=0}^{n-1} \frac{f(x,y)}{1+|x-y|} \quad \ldots\ldots. (28)$$

Table 1 presents the Overview of the parameters for 7 scans in table format. The parameters covered are Contrast, Correlation, Energy, Homogeneity, Mean, and Standard Deviation. Table 2 also presents the Overview of the other parameters for 7 scans in table format. The parameters covered are Entropy, RMS, Variance, Smoothness, Kurtosis, and Skewness & Inverse Different Moment (IDM).

Table 1. Overview of the parameters for 7 scans in table format

Image	Contrast	Correlation	Energy	Homogeneity	Mean	Standard Deviation
1	0,2539	0,1014	0,7610	0,9329	0,0017	0,0892
2	0,2258	0,1529	0,7689	0,9364	0,0017	0,0892
3	0,2152	0,1143	0,7526	0,9326	0,0048	0,0896
4	0,3167	0,1297	0,7949	0,9395	0,0075	0,0899
5	0,243	0,0943	0,7488	0,9300	0,0050	0,0897
6	0,23	0,0871	0,7513	0,9301	0,0046	0,0895
7	0,2364	0,1479	0,7429	0,9287	0,0046	0,0895

https://doi.org/10.56294/saludcyt2023434

Table 2. Overview of the parameters for 7 scans in table format

Image	Entropy	RMS	Variance	Kurtosis	Skewness	Inverse Different Moment (IDM)
1	2,9641	0,0898	0,0081	7,8474	0,5534	0,1548
2	3,0447	0,0897	0,0082	7,2954	0,3964	0,6042
3	3,7365	0,0868	0,0081	5,8455	0,4031	1,5651
4	3,1611	0,0892	0,0080	13,499	1,3523	0,8302
5	3,614	0,0892	0,0081	6,052	0,5247	1,1661
6	3,7295	0,0848	0,0082	5,6958	0,3829	0,5801
7	3,5494	0,0886	0,0081	6,573	0,6144	0,3837

The classification is required since the results from segmentation are inadequate. Nevertheless, we initially gather the feature extraction of the image. The trained data which we have is compared with the actual data. The trained data is matched to the various parameters. On basis of the data acquired from the result the categorization is carried out. The parameters analyse the train data and classify the picture depending on the textive features of the image. It is discovered using the parameters that determines whether the tumor is benign or a malignant.

CLASSIFICATION

In Classification the analysis of the presence or absence of tumor is implemented. It is presented in form of Confusion matrix.[20] It is a popular depiction for evaluating a classification technique's effectiveness. It may also be employed to examine the outcomes of a technique. The four Confusion matrix is presented below.

Table 3. Confusion Matrix

Total Images		Predicted	
		With Tumor	NO Tumor
Actual	With Tumor	TP	FN
	NO Tumor	FP	TN

The description of TP, TN, FP & FN are mentioned below:

- TP is True Positive and it comes when the image is having tumor then the output will also come tumor. The tumor can be either Benign or Malignant. The Input & Output can be in form of Benign - Benign, Malignant – Malignant etc.[10]
- TN is True Negative and it comes when the scan is not having tumor then output will come as NO Tumor. The Input & Output can be in form of NO Tumor - NO Tumor.
- FP is False Positive and it comes when the picture is having NO Tumor then output will come with tumor. The tumor can be either Benign or Malignant. The Input & Output can be in form of NO Tumor – with Tumor (either Benign or Malignant).
- FN is False Negative and it comes when the image is with tumor then output will come NO Tumor or wrong detection of Tumor. The tumor can be either Benign or Malignant. The Input & Output can be in form of Benign Tumor – NO Tumor, Benign Tumor – Malignant Tumor, Malignant Tumor - NO Tumor and Malignant Tumor - Benign Tumor.

Table 4. Confusion Matrix for using [(Weiner + Anistropic) + Cuckoo Otsu + DWT + SVM]

Total Images – 170 Tumor Images – 110 No Tumor Images - 60		Predicted	
		With Tumor	NO Tumor
Actual	With Tumor	TP (100)	FN (10)
	NO Tumor	FP (07)	TN (53)

In table 4, the Confusion Matrix for using (Weiner + Anistropic) +Cuckoo Otsu + DWT + SVM is implemented. It is seen that totally 170 images are taken into consideration. In this there are 110 are tumor images and 60 are non-tumor images. In the above table, TP is True Positive, TN means True Negative, FP denotes as False Positive & FN signifies as False Negative. Here TP=100, FN=10, FP=7 & TN=53 respectively.

Table 5. Confusion Matrix for using [(Weiner + Anistropic) + Cuckoo Kapur + DWT + SVM]

Total Images - 170 Tumor Images - 110 No Tumor Images - 60		Predicted: With Tumor	Predicted: NO Tumor
Actual	With Tumor	TP (103)	FN (07)
	NO Tumor	FP (05)	TN (55)

In table 5, the Confusion Matrix for using (Weiner + Anistropic) + Cuckoo Kapur + DWT + SVM is implemented. It is seen that totally 170 images are taken into consideration. In this there are 110 are tumor images and 60 are non-tumor images. Here TP=103, FN=7, FP=5 & TN=55 respectively.

Table 6. Confusion Matrix for using [(Weiner + Anistropic) + Cuckoo Tsallis + DWT + SVM]

Total Images - 170 Tumor Images - 110 No Tumor Images - 60		Predicted: With Tumor	Predicted: NO Tumor
Actual	With Tumor	TP (106)	FN (04)
	NO Tumor	FP (04)	TN (56)

In table 6, the Confusion Matrix for using (Weiner + Anistropic) + Cuckoo Tsallis + DWT + SVM is implemented. It is seen that totally 170 images are taken into consideration. In this there are 110 are tumor images and 60 are non-tumor images. Here TP=106, FN=4, FP=4 & TN=56 respectively.

Table 7. Confusion Matrix for using [(Weiner + Anistropic) + Cuckoo combined {Ostu + Tsallis } + DWT + SVM]

Total Images - 170 Tumor Images - 110 No Tumor Images - 60		Predicted: With Tumor	Predicted: NO Tumor
Actual	With Tumor	TP (108)	FN (02)
	NO Tumor	FP (03)	TN (57)

In table 7, the Confusion Matrix for using proposed method (Weiner + Anistropic) + Cuckoo combined {Ostu + Tsallis} + DWT + SVM is implemented. It is seen that totally 170 images are taken into consideration. In this there are 110 are tumor images and 60 are non-tumor images. Here TP=108, FN=2, FP=3 & TN=57 respectively. It is analyzed that from the above implemented methods, the Confusion Matrix for using [(Weiner + Anistropic) + Cuckoo combined {Ostu + Tsallis} + DWT + SVM gives the best possible outcome.

The confusion matrix of classification is presented above. There are five performance assessments that are being considered in the article. They are Sensitivity (Se), Specificity (Sp), Positive Predictive Value (PPV), Negative Predictive Value (NPV) & Accuracy (Acc).[12] The performance assessment of proposed system is analysed & their equations are presented below.

SENSITIVITY (SE)

Sensitivity is the ratio of True Positive to the combination of True Positive & False Negative. [10] The equation of Sensitivity is given by:

$$\text{Sensitivity}(S_e) = \frac{TP}{TP+FN} \quad \text{.......} \ (29)$$

SPECIFICITY (SP)

Specificity is the ratio of True Negative to the combination of False Positive & True Negative.
The equation of Specificity is given by:

$$\text{Specificity}(S_p) = \frac{TN}{FP+TN} \quad \text{........ (30)}$$

POSITIVE PREDICTIVE VALUE (PPV)

Positive Predictive Value is the ratio of True Positive to the combination of True Positive & False Positive [10]
The equation of Positive Predictive Value is given by:

$$PPV = \frac{TP}{TP+FP} \quad \text{....... (31)}$$

NEGATIVE PREDICTIVE VALUE (NPV)

Negative Predictive Value is the ratio of True Negative to the combination of True Negative & False Negative. [10] The equation of Positive Predictive Value is given by:

$$NPV = \frac{TN}{TN+FN} \quad \text{...... (32)}$$

ACCURACY (ACC)

Accuracy is the ratio of combination of True Positive & True Negative to the combination of True Positive, False Negative, and True Negative & False Positive.[10] The equation of Accuracy is given by:

$$\text{Accuracy} = \frac{TP+TN}{TP+FN+TN+FP} \quad \text{........ (33)}$$

Table 8. Different Methods with their respective parameters for tumor detection

Sr. No	Methods	Se	Sp	PPV	NPV	Acc
1	(Weiner + Anistropic) + Cuckoo Otsu+ DWT + SVM	0,909	0,8833	0,9345	0,8412	0,900
2	(Weiner + Anistropic) + Cuckoo Kapur + DWT + SVM	0,936	0,9166	0,9537	0,8870	0,929
3	(Weiner + Anistropic) + Cuckoo Tsallis + DWT + SVM	0,9636	0,9333	0,9636	0,9333	0,952
4	Proposed Method	0,981	0,9500	0,9729	0,9661	0,970

In table 8, five different parameters using confusion matrix are found for different methods. In first method, in the segmentation part, multi-thresholding cuckoo algorithm using ostu as an objective function used. In second method, in the segmentation part, multi-thresholding cuckoo algorithm using kapur entropy as an objective function used. In third method, in the segmentation part, multi-thresholding cuckoo algorithm using Tsallis entropy as an objective function used in the proposed multi-thresholding cuckoo algorithm combined ostu and Tsallis entropy used as an objective function that gives best output for all parameters.

CONCLUSION

The research activity consists of several stages, including Pre-processing, Segmentation, Feature Extraction and Classification. Individual and combinations of filters such as the Median, Weiner, Anisotropic, NLM, Weiner and NLM, Weiner and Anisotropic, and Weiner and Median have been described for the pre-processing process. Weiner and anisotropic filtering together produced the best results. Various thresholding, entropy, and evolutionary techniques, such as Two-level thresholding, Multilevel thresholding, Otsu's method, Kapur's entropy method, Tsallis entropy method & Cuckoo search (CS) algorithm, Lévy flight modelling are detailed in segmentation. It is observed that the Cuckoo Otsu & Tsallise Threshold combination delivers outstanding outcome in segmentation. In Feature Extraction Discrete Wavelet Transform (DWT) is used. One seventy images were considered for MRI scan and numerous parameters were discussed. Since Segmentation cannot generate an accurate outcome and hence Feature extraction is utilized. Based on textive feature of an image the parameters are compared to trained data and then its classification is done. Regarding Classification methodology Support vector machine (SVM) is described. The Confusion matrix and various filter combinations are deployed for detecting tumors. The parameters like Sensitivity, Specificity, Positive Predictive Value (PPV), Negative Predictive Value (NPV) & Accuracy (Acc) of combination of filters are compared with help of True Positive, True Negative, and False Positive & False Negative. The combination of (Weiner + Anistropic) + Cuckoo combined {Ostu+ Tsallis} + DWT

+ SVM deliver excellent result. The proposed methodology reflects the effective way to identify the nature of brain tumors along with adequate MRI scan.

REFERENCES

1. Bhavna Pancholi K, Pramod Modi S. Noise reduction in clinical MRI scans employing filter combining techniques. In: 2nd International Conference on Technological Advancements in Computational Sciences (ICTACS); 2022. IEEE conference proceedings.

2. Buades Coll B, Morel JM. A review of image denoising algorithms, with a new one. Multiscale Model Simul. 2005;4(2):490-530.

3. Chahal PK. A survey on brain tumor detection techniques for MR images. Multimedia Tools Appl. 2020;79(29-30):21771-21814. doi:10.1007/s11042-020-08898-3.

4. Nagarajan I, Lakshmi Priya GG. Removal of noise in MRI images using a block difference-based filtering approach. Int J Imaging Syst Technol. 2019;30(3):1203-1215. doi:10.1002/ima.22361.

5. Maheshan CM, Prasanna Kumar H. Performance of image pre-processing filters for noise removal in transformer oil images at different temperatures. SN Appl Sci. 2019;2(1):1. doi:10.1007/s42452-019-1800-x.

6. Gayathri S. Analyzing, detecting and automatic classification of different stages of brain tumor using region segmentation and support vector machine. In: 2020 International Conference on Electronics and Sustainable Communication Systems (ICESC); 2020. doi:10.1109/icesc48915.2020.9156057.

7. Jia Z, Chen D. Brain tumor identification and classification of MRI images using deep learning techniques. IEEE Access. 2020;8:108181-108189. doi:10.1109/access.2020.3016319.

8. Vadmal V, Junno GT, Badve C, Huang WC, Waite K, Barnholtz-Sloan JS. MRI image analysis methods and applications: an algorithmic perspective using brain tumors as an exemplar. Neuro Oncol Adv. 2020;2(1):vdaa049. doi:10.1093/noajnl/vdaa049.

9. Raut AM. Texture parameters extraction of satellite image. IJSTE Int J Sci Technol Eng. 2016;2(11).

10. Yang XS, Deb S. Cuckoo search via Lévy flights. In: 2009 World Congress on Nature & Biologically Inspired Computing (NaBIC); 2009.

11. Deng Q. Self-adaptive image thresholding within nonextensive entropy and the variance of the gray-level distribution. Entropy. 2022;24(3):319. doi:10.3390/e24030319.

12. Kalpana R, Chandrasekar P. An optimized technique for brain tumor classification and detection with radiation dosage calculation in MR image. Microprocess Microsyst. 2020;72:102903. doi:10.1016/j.micpro.2019.102903.

13. Jude Hemanth D, Anitha J. Image pre-processing and feature extraction techniques for magnetic resonance brain image analysis. Commun Comput Inf Sci. 2012;349-356. doi:10.1007/978-3-642-35594-3_47.

14. Çinar A, Yildirim M. Detection of tumors on brain MRI images using the hybrid convolutional neural network architecture. Med Hypotheses. 2020;139:109684. doi:10.1016/j.mehy.2020.109684.

15. Mahmud Boby, Shakil, Sharmin S. Medical image denoising techniques against hazardous noises: An IQA metrics-based comparative analysis. Int J Image Graph Signal Process. 2021;13(2):25-43. doi:10.5815/ijigsp.2021.02.03.

16. Perona P, Malik J. Scale-space and edge detection using anisotropic diffusion. IEEE Trans Pattern Anal Mach Intell. 1990;12(7):629-639. doi:10.1109/34.56205.

17. Khairuzzaman AKM, Chaudhury S. Masi entropy-based multilevel thresholding for image segmentation. Multimed Tools Appl. 2019;78(23):33573-33591. doi:10.1007/s11042-019-08117-8.

18. Rahaman J, Sing M. An efficient multilevel thresholding-based satellite image segmentation approach using a new adaptive cuckoo search algorithm. Expert Syst Appl. 2021;174:114633. doi:10.1016/j.eswa.2021.114633.

19. Suresh S, Lal S. An efficient cuckoo search algorithm-based multilevel thresholding for segmentation of satellite images using different objective functions. Expert Syst Appl. 2016;58:184-209. doi:10.1016/j.eswa.2016.03.032.

20. Ou C. Generalized measure of uncertainty and the maximizable entropy. Mod Phys Lett B. 2010;24(9):825-831. doi:10.1142/s0217984910022883.

21. Tsallis C. Possible generalization of Boltzmann-Gibbs statistics. J Stat Phys. 1988;52(1-2):479-487. doi:10.1007/bf01016429.

22. Ramírez-Reyes A. Determining the entropic index Q of Tsallis entropy in images through redundancy. Entropy. 2016;18(8):299. doi:10.3390/e18080299.

23. Kapur JN. A new method for gray-level picture thresholding using the entropy of the histogram. Comput Vis Graph Image Process. 1985;29(3):273-285. doi:10.1016/0734-189x(85)90125-2.

24. Otsu N. A threshold selection method from gray-level histograms. IEEE Trans Syst Man Cybern. 1979;9(1):62-66.

25. Huang Z. The available force in long-duration memory complex systems and its statistical physical properties. EPL (Europhysics Letters). 2013;103(1):10011. doi:10.1209/0295-5075/103/10011.

26. Anoop V. Medical image enhancement by a bilateral filter using optimization technique. J Med Syst. 2019;43(8):240. doi:10.1007/s10916-019-1370-x.

CONFLICTS OF INTEREST

None.

FINANCING

No financing.

AUTHORSHIP CONTRIBUTION

Conceptualization: Bhavna Kaushik Pancholi, Pramodkumar Sevantilal Modi, Nehal Gitesh Chitaliya.

Research: Bhavna Kaushik Pancholi, Pramodkumar Sevantilal Modi, Nehal Gitesh Chitaliya.

Writing - proofreading and editing: Bhavna Kaushik Pancholi, Pramodkumar Sevantilal Modi, Nehal Gitesh Chitaliya.